Research on wind erosion processes and controlling factors based on wind tunnel test and 3D laser scanning technology

YAN Ping[1,2], WANG Xiaoxu[1,3,4*], ZHENG Shucheng[1,3], WANG Yong[5], LI Xiaomei[6]

[1] Faculty of Geographical Science, Beijing Normal University, Beijing 100875, China;
[2] Zhuhai Branch of State Key Laboratory of Earth Surface Processes and Resource Ecology, Beijing Normal University, Zhuhai 519087, China;
[3] State Key Laboratory of Earth Surface Processes and Resource Ecology, Beijing Normal University, Beijing 100875, China;
[4] MOE Engineering Research Centre of Desertification and Blown-sand Control, Beijing 100875, China;
[5] Institute of Geographical Sciences, Henan Academy of Sciences, Zhengzhou 450052, China;
[6] School of Geography and Tourism, Shaanxi Normal University, Xi'an 710119, China

Abstract: The study of wind erosion processes is of great importance to the prevention and control of soil wind erosion. In this study, three structurally intact soil samples were collected from the steppe of Inner Mongolia Autonomous Region, China and placed in a wind tunnel where they were subjected to six different wind speeds (10, 15, 17, 20, 25, and 30 m/s) to simulate wind erosion in the wind tunnel. After each test, the soil surfaces were scanned by a 3D laser scanner to create a high-resolution Digital Elevation Model (DEM), and the changes in wind erosion mass and microtopography were quantified. Based on this, we performed further analysis of wind erosion-controlling factors. The study results showed that the average measurement error between the 3D laser scanning method and weighing method was 6.23% for the three undisturbed soil samples. With increasing wind speed, the microtopography on the undisturbed soil surface first became smooth, and then fine stripes and pits gradually developed. In the initial stage of wind erosion processes, the ability of the soil to resist wind erosion was mainly affected by the soil hardness. In the late stage of wind erosion processes, the degree of soil erosion was mainly affected by soil organic matter and $CaCO_3$ content. The results of this study are expected to provide a theoretical basis for soil wind erosion control and promote the application of 3D laser scanners in wind erosion monitoring.

Keywords: 3D laser scanning technology; wind erosion; wind tunnel test; wind erosion depth; microtopography; soil hardness

Citation: YAN Ping, WANG Xiaoxu, ZHENG Shucheng, WANG Yong, LI Xiaomei. 2022. Research on wind erosion processes and controlling factors based on wind tunnel test and 3D laser scanning technology. Journal of Arid Land, 14(9): 1009–1021. https://doi.org/10.1007/s40333-022-0103-z

1 Introduction

Soil wind erosion is one of the most severe environmental problems in arid and semi-arid areas throughout the world (Lyu et al., 2021; Zhao et al., 2021). It is not only a primary and important aspect of wind and sand dynamics and desertification, but also one of the basic geomorphic processes that shape the Earth's landscape (Cooke et al., 1993). Soil erosion is a major cause of global terrestrial soil degradation and threatens freshwater and ocean environments (Borrelli et

*Corresponding author: WANG Xiaoxu (E-mail: 202131051012@mail.bnu.edu.cn)
Received 2022-06-13; revised 2022-07-28; accepted 2022-08-20

al., 2020; Ferreira et al., 2022). The core mechanisms of wind erosion processes involve the separation, transportation, and deposition of soil particles, as well as the variable dynamics of each wind erosion factor and the mutual feedback relationships among them (Zhang et al., 2018). Researchers divided the factors affecting wind erosion processes into three categories based on wind erosion dynamics, including air factors, surface factors, and soil factors (Chepil, 1945). The surface factors include surface roughness and topography, and the soil factors contain soil structure and moisture content. For the surface factors, microtopography is an important factor controlling aerodynamic roughness and shear stress distribution (Kardous et al., 2005); as such, its influence on soil wind erosion processes cannot be ignored. Soil structure (including soil organic matter, $CaCO_3$, and mechanical composition) significantly affects the critical wind speed and wind erosion rate of soil (Guerrero et al., 2021; Mozaffari et al., 2021). The wind erosion amount is an important index to judge the intensity of soil wind erosion and desertification. It is widely used in the research of wind erosion-related issues (Sterk et al., 1999; Wang et al., 2019). The methods of measuring the soil wind erosion amount mainly include field investigations and observations, wind tunnel simulation tests, and wind erosion models. The main methods of external measurement are sampler collection method, particle size comparison method (Wang et al., 2013), erosion pins method (Haigh, 1977; Gupta et al., 1981), and wind erosion traces (Dunne et al., 1978; Carrara and Carroll, 1979). The erosion pins method can only indicate the wind erosion amount occurring over a long time interval, while the collection efficiency of the sand sampler is low and is affected by uncertain factors such as surface uniformity. The wind tunnel simulation tests have become an important mean to study the wind erosion rate due to controllable conditions (Zhang et al., 2006), though these simulations lack real soil and atmospheric environments and have difficulty satisfying the requirements of these criteria. At present, the commonly used wind erosion models include Wind Erosion Equation, Texas Erosion Analysis Model, Revised Wind Erosion Equation, and Wind Erosion Prediction System. While these models are based on a large number of observations and experiments, their accuracy needs to be further verified, and problems of universality remain. Considering this, it is critical to study wind erosion processes and to improve the measurement accuracy of soil surface microtopography and the wind erosion amount.

3D laser scanning technology, also known as "reality replication technology", uses noncontact high-speed laser measurement technology to obtain image data and map the topography or complex objects. The measurement principle, application, development, and accuracy tests have been reviewed by Jaboyedoff et al. (2012) and Soudarissanane et al. (2011). In recent years, 3D laser scanning technology has been widely used in engineering (Cheng and Jin, 2006), archaeology (Kuzminsky and Gardiner, 2012; Polig, 2017), and medicine (Kovacs et al., 2006; Sansoni et al., 2009). Since 3D laser scanning technology has matured, it has become widely used in the study of aeolian processes. Nield et al. (2013) used terrestrial laser scanning to characterize the roughness of typical dust-emitting surfaces and found that any metric based on feature protrusion height has an increased likelihood of successfully predicting terrain roughness. This finding has good implications for the development of wind erosion and dust emission studies. Nagihara et al. (2004) tested the feasibility of using a 3D laser scanner to quickly obtain highly accurate topographic surveys of dunes, and the spatial resolution of 3D laser scanner can constrain the mathematical model of dune evolution. Ding et al. (2009) measured the change in the micromorphology of erosion deposits in a straw checkerboard barrier with a 3D laser scanner. This verified the feasibility of monitoring microtopographic changes with 3D laser scanning technology and supported the belief that the technique had unique advantages in dune migration monitoring and sand management. Pelletier et al. (2015) measured the mean critical and repose angles and the rate of slip-face avalanching using terrestrial laser scanning on two barchans of different sizes in Jericoara, Brazil, and combined with wind speed data, they found that the mean critical angle decreased with increasing wind speed. An et al. (2017) studied the application of a 3D laser scanner in the observation of aeolian landforms and proposed an observation scheme for aeolian landforms. The reliability of this method was tested by comparing it with traditional

measuring equipment. Cheng et al. (2017) used a 3D laser scanner to monitor the changes in a sand bed before and after each experiment at three friction velocities. Based on this approach, they studied sand morphological surface development, and described the evolution of the wind erosion rate as a function of distance. It is of critical importance to study the effect of sand bed length on the mass of material displaced by wind erosion. Bhutto et al. (2022) observed the changes in the surface microtopography resulting from erosion and sediment deposition around four plants and found that plants were able to capture the displaced sediment that was eroded from the upwind area.

The process of soil wind erosion is a relatively complex process affected by the soil structure. In this study, we compared the 3D laser scanning results of wind tunnel test conducted on three undisturbed soils in the Xilin Gol grassland and, using weighing method, quantitatively analyzed and evaluated the accuracy of 3D laser scanning technology in measuring wind erosion. In addition, based on 3D laser scanning technology, we expound the change in microtopography with the intensity of wind erosion and the influence of soil hardness, soil organic matter, and $CaCO_3$ content on soil wind erosion. The results can provide a theoretical basis for soil wind erosion prevention and promote the application of 3D laser scanners in wind erosion monitoring.

2 Materials and methods

2.1 Experimental preparation

In May 2018, undisturbed soils from three regions (S1, S2, and S3) were collected in the Xilin Gol grassland, Inner Mongolia Autonomous Region of China (Fig. 1). Each soil sample was cut into pieces and placed in a wooden box with 80 cm×30 cm×15 cm, covered with fresh-keeping film, sealed and bound with iron wire to prevent contamination and damage during transportation. Before the experiment, the roots, plant debris, and stones within 5 cm of the surface layer were removed. The samples were watered multiple times prior to extraction, and dried naturally to restore them to the original soil state. In addition, soil moisture, bulk density, soil hardness, soil organic matter, and $CaCO_3$ content of the three soil samples were measured (Table 1).

Fig. 1 Soil sampling process in the field

Table 1 Basic properties of the three soil samples

Sample	Region	Location	Altitude (m)	Soil type	Soil moisture (%)	Bulk density (g/cm^3)	Soil hardness (kPa)	$CaCO_3$ content (%)	Soil organic matter (%)
S1	Baoligen Sumu, Xilinhot City	44°14′50″N, 115°56′27″E	948	Meadow kastanozem (Calciustolls)	2.07	1.45	19.30	9.84	2.14
S2	Longchang Town, Chifeng City	43°49′44″N, 119°49′10″E	434	Dark kastanozem (Calciustolls)	2.14	1.38	7.35	4.85	1.28
S3	Fuhe Town, Chifeng City	44°30′28″N, 119°10′44″E	782	Sandy chernozem (Argiborolls)	3.47	1.29	19.40	0.22	2.44

2.2 Wind tunnel test and 3D laser scanning technology

The wind tunnel test was performed in the Wind Sand Environment and Engineering Laboratory of Beijing Normal University (Fig. 2). The wind tunnel has a length of 37 m, a test section of 16 m, and a cross section of 1 m high and 1 m wide, with wind speeds ranging from 3 to 45 m/s and a pulsation less than 1%. The soil samples were placed on the center of the test section using a manual lift to keep the soil surface at the same height as the floor of the wind tunnel. We used a 3D laser scanner (Trimble GX DR 200+, Trimble Inc., State of California, USA) with a scanning scope of 200–350 m. The distance between scanning points was set to 1.00 mm.

The wind speed in the center of the test section was set as follows: 10, 15, 17, 20, 25, and 30 m/s. Except for the wind speed of 10 m/s, which had an erosion time of 10 min, the erosion time for all other wind speeds was 5 min. The soil surface was scanned by opening the observation window before and after each erosion test. Then, the soil trough was removed and weighed with an electronic scale (KCC150, Mettler-Toledo, Zurich, Switzerland) (Fig. 2c) to measure wind erosion mass (W_{ab}).

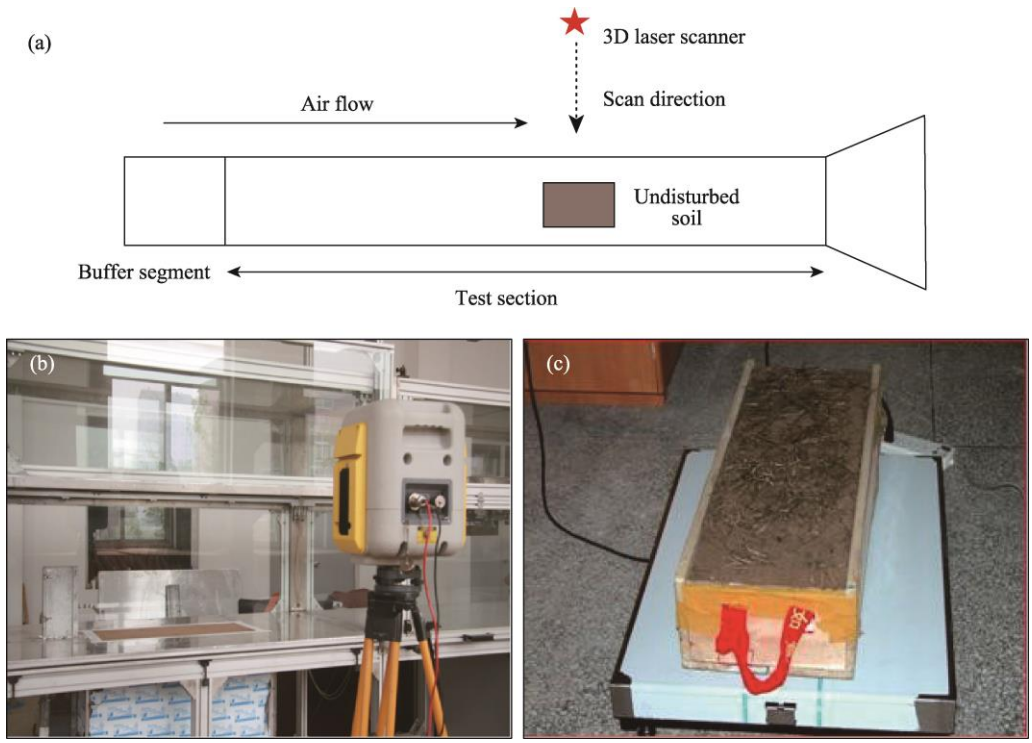

Fig. 2 Experimental operation diagram. (a), the schematic diagram of experimental layout; (b), the photo of experimental operation; (c), the photo of soil weighing method.

2.3 Data analysis

The point cloud data (soil trough frame and soil surface) obtained from each scan were processed by the scanning software Realworks 6.5, converted into dwg format files and imported into ArcGIS. The scanner automatically generates a coordinate system with its internal center as the origin. We converted the scans into Digital Elevation Model (DEM) images in ArcGIS to calculate the average height. It should be noted that after each erosion test, the box needed to be removed for weighing. Since relatively fixed targets cannot be installed in the soil, the wood frame surface was used as the datum for data alignment. The calculation formula of wind erosion depth (D_{ab}; mm) after each erosion test was as follows:

$$D_{ab} = (H_{ab} - h_{ab}) - (H_{a0} - h_{a0}), \tag{1}$$

where H_{ab} is the height of the soil surface (mm); h_{ab} is the height of the soil trough frame (mm); a represents the number of soil samples (1, 2, and 3); b represents the number of each wind speed (10, 15, 17, 20, 25, and 30 m/s); and 0 represents the initial conditions.

The formula for determining the wind erosion mass from the 3D laser scanning (M_{ab}; g) was as follows:

$$M_{ab} = (D_{ab} \times 80 \times 30 \times Bd_a) / 10, \tag{2}$$

where Bd_a is the soil bulk density (g/cm^3).

Based on the wind erosion mass measured by weighing method (W_{ab}; g), we calculated the relative error of the wind erosion mass (ξ_{ab}; %) obtained from each scanning test using the following equation:

$$\xi_{ab} = 100\% \times |M_{ab} - W_{ab}| \times W_{ab}. \tag{3}$$

Root mean squared height (RMSH; mm) is a commonly used calculation index to describe soil surface roughness (Eitel et al., 2011; Nield et al., 2011; Nield et al., 2013), and the calculation formula was as follows:

$$\mathrm{RMSH} = \sqrt{\frac{\sum_i^n (z_i - \mu)^2}{n-1}}, \tag{4}$$

where z_i is the height within each grid cell included in the moving window (mm); μ is the mean elevation within the moving window (mm); and n is the number of grid cells within the moving window.

3 Results and analysis

3.1 Comparison between 3D laser scanning technology and weighing method

The soil sample was removed from the wind tunnel after each test and placed on an electronic scale to accurately weigh the wind erosion mass (Fig. 2c). This process is called "weighing method", which is a more direct and accurate method to obtain the wind erosion mass in the laboratory. The wind erosion masses determined by 3D laser scanning technology and weighing method are compared in Table 2. Under the wind speeds of 15, 17, 20, and 30 m/s, the relative errors of the two methods for S1 were 0.51%, 21.73%, 15.90%, and 12.03%, respectively, the average relative error was 10.05%, and the relative error of cumulative wind erosion mass was 10.20%. The relative error range of S2 under each wind speed was 2.85%–11.06%, the average relative error was 6.63%, and the relative error of cumulative wind erosion mass was 1.65%. Except for the relative error in S3 under the wind speed of 10 m/s, the relative errors under other wind speeds were small and the relative error of cumulative wind erosion mass was 7.00%. The overall average relative error was 14.07%.

Table 2 Comparison between 3D laser scanning technology and weighing method

Wind speed (m/s)	S1			S2			S3		
	D (mm)	*W* (g)	*ξ* (%)	*D* (mm)	*W* (g)	*ξ* (%)	*D* (mm)	*W* (g)	*ξ* (%)
10	0.00	0.00	0.00	0.65	230.28	6.51	0.01	4.68	33.85
15	0.18	62.96	0.51	3.70	1191.44	2.85	0.65	224.21	10.24
17	0.59	262.32	21.73	2.21	822.93	11.06	0.98	284.40	6.68
20	3.39	1017.51	15.90	2.22	816.21	9.92	2.54	717.23	9.64
25	-	-	-	4.19	1302.71	6.53	1.68	471.12	10.40
30	5.64	1752.01	12.03	0.84	287.02	3.07	1.03	291.88	9.25
Total	9.80	3094.80	10.20	13.81	4650.89	1.65	6.89	1993.52	7.00

Note: *D*, wind erosion depth; *W*, wind erosion mass; *ξ*, relative error; -, no data.

3.2 Development process of microtopography

Microtopography refers to the relative elevation changes in the soil surface at scales of millimeters to centimeters caused by soil particles, aggregates, soil blocks, tillers, etc. The changes in the microtopography of the undisturbed soil surface increased as the wind speed and test time increased (Fig. 3). Taking S3 as an example (Fig. 4), under the wind speeds of 10 and 15 m/s, the wind erosion mass was 224.21 g, the wind erosion depth was 0.65 mm, and there was no typical wind scour pattern on the soil surface. When the wind speed reached 17 m/s, the wind erosion mass increased to 284.40 g, the wind erosion depth increased by 0.98 mm, and small scour pits appeared on the soil surface. After being subjected to a wind speed of 20 m/s, 717.23 g of topsoil was displaced, and the wind erosion depth increased by 2.54 mm. A pit with a wind erosion depth of approximately 8.00 mm appeared in the part of the sample and had a wind erosion area of approximately 5434 mm^2. There were discontinuous small pits in the middle of the larger erosional pit, which had a total wind erosion area of 652 mm^2 and was the evidence of a strong wind erosion area. Under the wind speed of 25 m/s, the pit expanded and deepened, and a groove appeared in the front. In the front of the groove, a new long and narrow pit developed. The pit was more obvious than before, with a wind erosion area of approximately 384 mm^2, an average wind erosion depth of 4.00 mm, and a volume of 82,324 mm^3. When the wind speed accelerated to 30 m/s, erosion mainly occurred near the scour pit and groove. The area of the pit increased, the wind erosion depth increased, the wind erosion area was approximately 618 mm^2, the average wind erosion depth decreased by 1.03 mm, and the volume of the pit was 82,204 mm^3. Additionally, the wind scour groove was connected with the pit, and a pit with a wind erosion depth of approximately 6.00 mm was also produced in the upwind direction. With the increase of the wind speed, the groove and pit on the soil surface continued to deepen and broaden.

We selected the deepest area of the sample shown in Figure 4g and analyzed the change in the soil erosion depth along the horizontal direction in detail (Fig. 5). The surface of undisturbed soil was not smooth, especially when the horizontal position of the undisturbed soil was 25.00, 130.00, 410.00 mm (the horizontal beginning of the soil samples that along the upwind side was annotated as 0.00 mm), there was obvious peaks. Under the wind speed of 10 m/s, the wind erosion depth of the above three positions decreased significantly, and the wind erosion depth at the horizontal position of 410.00 mm decreased by about 5.00 mm, showing an obvious concave shape. The surface of the soil samples became relatively flat. First, at the horizontal position of 0.00–400.00 mm, the microtopography fluctuation changes were minimal as the wind speed increased. The higher part of the terrain at the horizontal position of 400.00–800.00 mm underwent considerable wind erosion, while the lower part of the terrain experienced only light wind erosion, and the wind erosion depth increased. When the wind speed was 17 m/s, the wind erosion depth decreased slightly due to the small change in the wind speed gradient, which was similar to the change in the wind speed of 15 m/s. When the wind speed increased to 20 m/s, the wind erosion depth at horizontal position of 0.00–250.00 mm was reduced, and the change in the wind erosion depth was

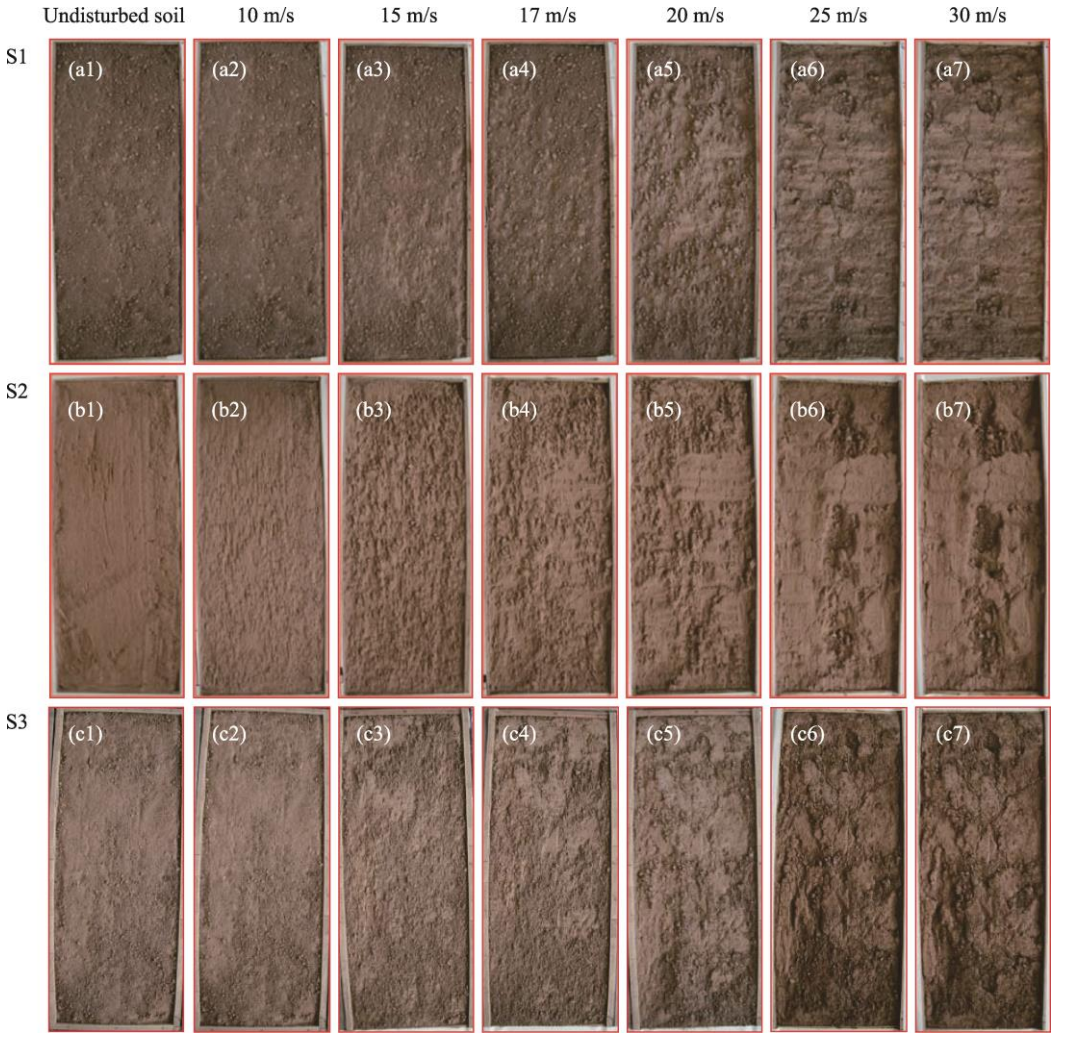

Fig. 3 Surface morphology of three samples (S1, S2, and S3) under different wind speed. (a1, b1, and c1), undisturbed soil; (a2, b2, and c2), wind speed of 10 m/s; (a3, b3, and c3), wind speed of 15 m/s; (a4, b4, and c4), wind speed of 17 m/s; (a5, b5, and c5), wind speed of 20 m/s; (a6, b6, and c6), wind speed of 25 m/s; (a7, b7, and c7), wind speed of 30 m/s.

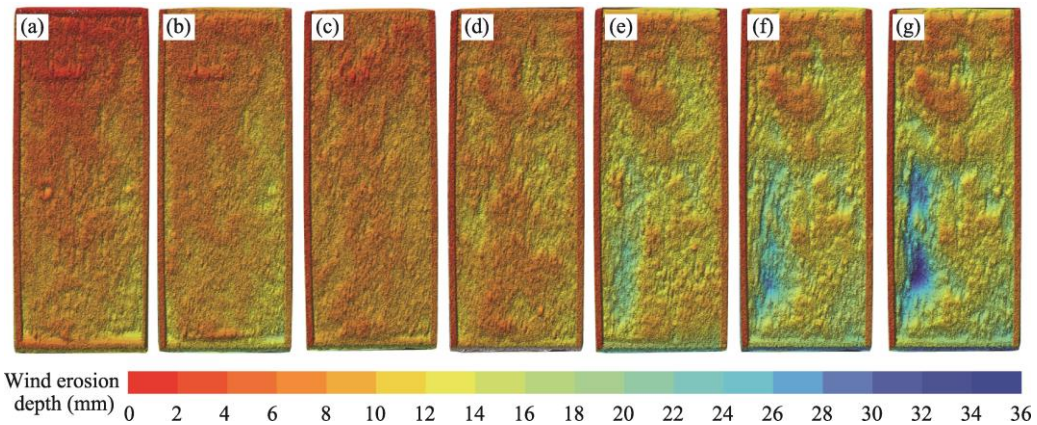

Fig. 4 Digital Elevation Model (DEM) images of the wind erosion depth generated in ArcGIS under different wind speed. (a), undisturbed soil; (b), wind speed of 10 m/s; (c), wind speed of 15 m/s; (d), wind speed of 17 m/s; (e), wind speed of 20 m/s; (f), wind speed of 25 m/s; (g), wind speed of 30 m/s.

small. At the horizontal position of 250.00–500.00 mm, the wind erosion depth increased, but it had little impact on the variability of the microtopography surface.

The horizontal position of 500.00–800.00 mm experienced strong wind erosion, and the maximum wind erosion depth reached 22.00 mm. Under the wind speed of 25 m/s, the wind erosion depth at horizontal position of 250.00–800.00 mm increased significantly. The horizontal position of 500.00 mm contained a groove scoured by the wind, which was divided into two large pits. The pit in the upwind direction was small, the difference in the wind erosion depth was small, the bottom was relatively flat, and the maximum wind erosion depth was 20.00 mm. The wind erosion depth of the pit in the downwind direction was 28.00 mm. When the wind speed reached 30 m/s, the pit continuously deepened and widened, and the maximum wind erosion depth was approximately 35.00 mm. As the erosion processes continued, the soil surface first became smooth and then gradually became rough (Fig. 6). Under the wind speeds of 10, 15, and 17 m/s, the soil surface was in a "consolidation" stage, loose soil particles and small aggregates were eroded, RMSH and the surface roughness decreased. When the wind speed was greater than 20 m/s, the wind speed increased, and large wind erosion areas appeared, with a RMSH of 4.67 mm. With the increase of wind speed, wind erosion mainly occurred near the large wind erosion areas, which further increased the wind erosion depth and increased the surface roughness of the soil. Under the wind speed of 30 m/s, the RMSH reached 6.80 mm, which was three times that of the undisturbed soil surface.

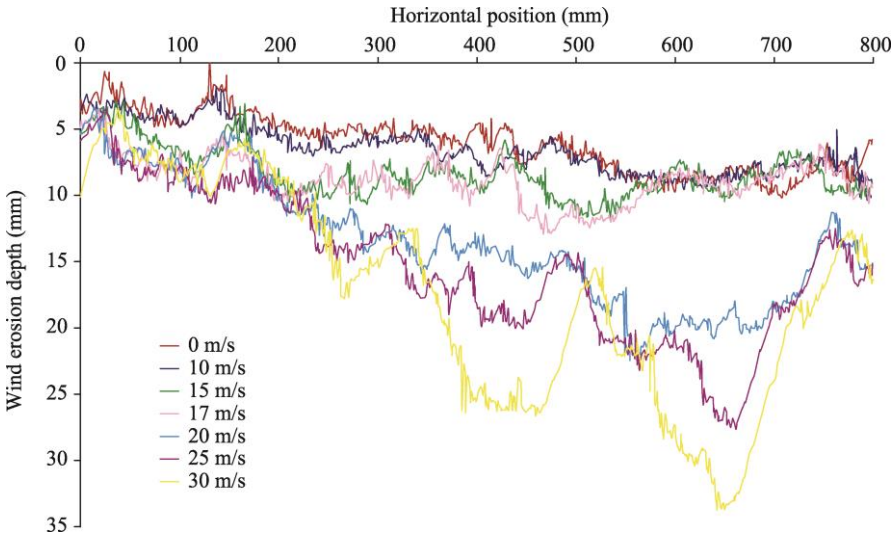

Fig. 5 Wind erosion depth along the horizontal position under different wind speed in S3

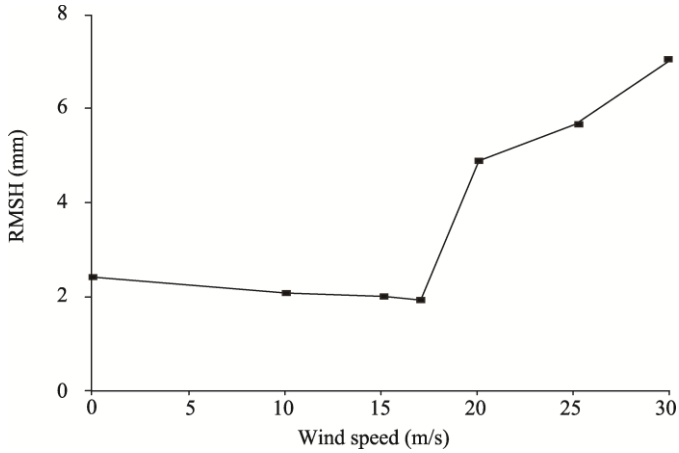

Fig. 6 Relationship between root mean squared height (RMSH) and wind speed

3.3 Differences in the wind erosion depth among different soil samples

The microstructural changes of the three samples were consistent. With the increase of wind speed, the microtopography on the undisturbed soil surface first became flat and then gradually developed into fine stripes and wind scour pits began to form (Fig. 3). The specific difference in microtopography was mainly reflected in the wind erosion depth. As shown in Figure 7, under the wind speed of 10 m/s, after 10 min, soil erosion occurred first in S2, and the wind erosion depth reached 0.65 mm. Only slight erosion changes occurred in the other two soil samples (S1 and S3). With the increase of wind speed, the wind erosion depth increased gradually, and the increase of wind erosion depth in S1 was the most obvious. When the wind speed reached 30 m/s, the wind erosion depth in S1 reached 5.64 mm. In S2, under the wind speeds of 17 and 20 m/s, the change in wind erosion depth was small. When the wind speed increased to 25 m/s, the wind erosion depth increased rapidly, and when the wind speed reached 30 m/s, the wind erosion depth decreased, which may be due to the decrease in erodible particles. When the wind speed reached 20 m/s, the wind erosion depth in S3 was 2.54 mm. Then, with the increase of wind speed, the variation in the wind erosion depth was decreased. Finally, the cumulative wind erosion depth in S1, S2, and S3 was 9.80, 13.81, and 6.89 mm, respectively. The wind erosion depth in S2 was the most pronounced, followed by S1.

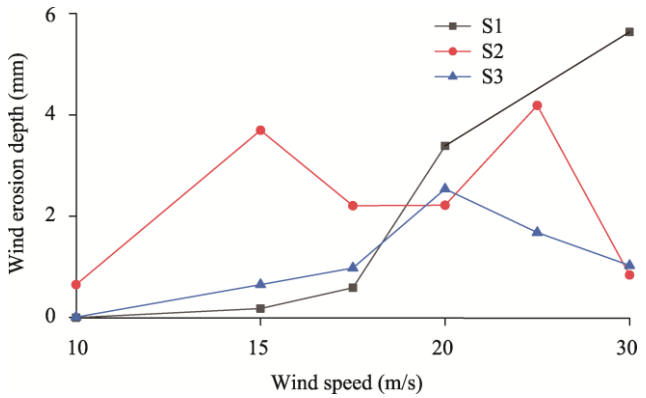

Fig. 7 Differences in the wind erosion depth among different soil samples. S1, S2, and S3 refer to sample number.

4 Discussion

4.1 Relative error analysis of 3D laser scanning technology

The error level is mainly related to the wind erosion depth and the accuracy of the scanner. We analyzed the cumulative wind erosion depth and relative error of the three samples and found that when the wind erosion depth exceeded the scanning accuracy, the relative error decreased (Fig. 8). In this study, when the wind erosion depth was greater than 1.40 mm, the relative error tended to be less than 10.00%. The minimum relative error was 1.08%, and the average error was 4.84%. When the wind erosion depth was less than 1.40 mm, the maximum error was 33.84%, and the average relative error was 13.84%. In addition, the surface roughness and the external temperature and pressure also caused measurement errors (Zheng et al., 2005). When the surface roughness increased to a certain extent, the measurement error increased. In recent years, 3D laser scanning technology has made great progress, and the accuracy of the new generation of 3D laser scanners has also been greatly improved. The resolution of the new scanners can reach 1.00 mm, and the scanning speed is faster (Zhao et al., 2022; Zhou et al., 2022). The 3D laser scanning technologies have matured and have obvious advantages in observing morphological structures (Wu et al., 2018; Zheng et al., 2021). Therefore, it is feasible and effective to measure wind-driven erosion with 3D laser scanning technology (Cheng et al., 2017; Asensio et al., 2019).

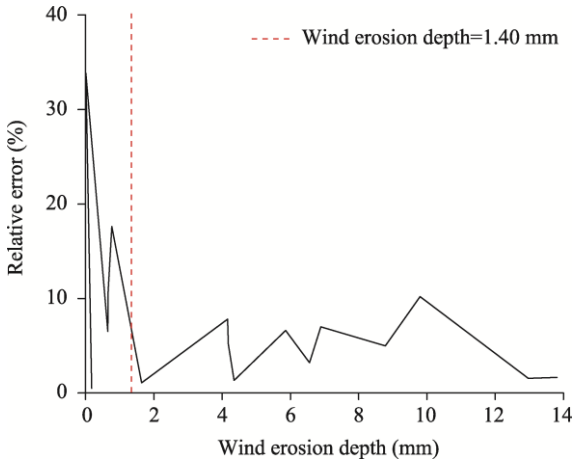

Fig. 8 Relationship between relative error and wind erosion depth

4.2 Effect of sample properties on soil wind erosion

The overall microtopographical changes of the three soil samples are the same, but there are certain differences in wind erosion mass and wind erosion depth, which are related to soil organic matter and $CaCO_3$ content (Fig. 9). After 10-min wind erosion, under the wind speed of 10 m/s, S1 and S3 barely experienced any erosion. The wind erosion depth in S2 increased by 0.65 mm, and the wind erosion mass was 230.28 g, which may be affected by the soil hardness. The soil hardness in S1, S2, and S3 is 19.30, 7.35, and 19.40 kPa, respectively. The soil hardness is one of the important physical properties of soil and is a comprehensive indicator of soil physical and chemical composition. The ability of soil to resist wind erosion is strongly influenced by the soil hardness (Li et al., 2003, 2005; Zhang et al., 2019). The greater the soil hardness, the greater the resistance to the incoming wind speed. With the increase of the wind speed, both the cumulative wind erosion depth and the wind erosion mass increased. After all tests were completed, the cumulative wind erosion depth in S1, S2, and S3 was 9.80, 13.81, and 6.89 mm, respectively, and the cumulative wind erosion mass in S1, S2, and S3 was 3094.80, 4650.89, and 1993.52 g, respectively. These differences are inferred to be related to the soil organic matter and $CaCO_3$ content in the three soil samples. Soil organic matter can improve the physical and chemical properties of soil and affect the susceptibility of soils to wind erosion (Münch et al., 2022). An increase in soil organic matter can enhance the ability of soil to resist wind erosion, and soil organic matter is positively correlated with resistance to wind erosion (Yuan et al., 2007; Jouquet et al., 2021). The soil organic matter in S1, S2, and S3 are 2.14%, 1.28%, and 2.44%, respectively, thus the wind erosion resistance in S2 is relatively weak. Areas with high $CaCO_3$ content are more susceptible to wind erosion than the areas with low $CaCO_3$ content, and a linear negative correlation between wind erosion rate and $CaCO_3$ content is considered in the United States Department of Agriculture Revised Wind Erosion Equation (Dong et al., 2018). $CaCO_3$ content in S1, S2, and S3 is 9.84%, 4.85%, and 0.22%, respectively. In this study, there is no significant correlation between $CaCO_3$ content and the wind erosion mass. We believe that this may be because the $CaCO_3$ content in the undisturbed soil did not play a role in wind erosion processes during the specified wind erosion time. S2 was more susceptible to wind erosion, followed by S1. The increase of the soil hardness, soil organic matter, and $CaCO_3$ content can increase soil resistance to wind erosion (Tian et al., 2018; Fallahzade et al., 2020; Sun et al., 2021).

4.3 Analysis of wind erosion processes of undisturbed soil

As a dynamic roughness element, the microtopography formed by uneven surface erosion is an important factor controlling the aerodynamic roughness of the surface. During the wind erosion processes, the pattern of convex parts and the accumulation of local pits make the microtopography always in a state of change (Kardous et al., 2005; Zhang et al., 2018). Soil erosion is a destructive

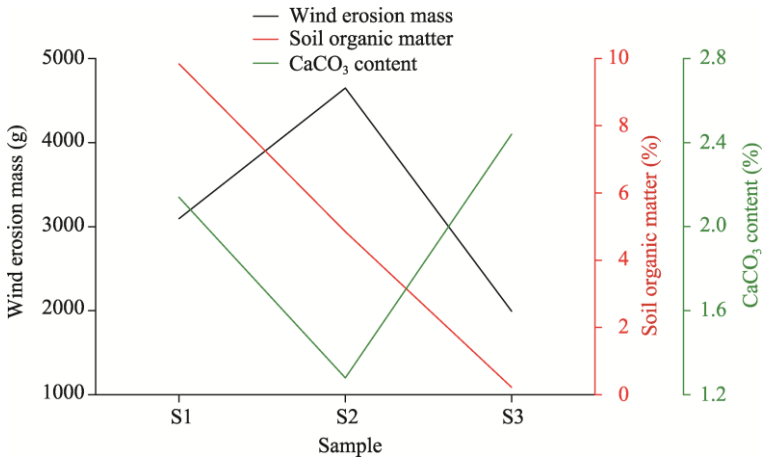

Fig. 9 Relationship of wind erosion mass with soil organic matter and $CaCO_3$ content

process that attacks the most productive topsoil layer first (Toy et al., 2002). In the wind tunnel test, the undisturbed soil is in the "soil preparation" stage during the early stage of wind erosion. The loose soil and small aggregates on the soil surface are first blown away, and the microtopography on the undisturbed soil surface initially becomes smooth. When the wind speed increases to 20 m/s, fine stripes and pits gradually develop on the soil surface. With the increase of wind speed, wind erosion mainly occurs in the vicinity of the grooves and pits, and the pits continue to deepen and widen. The roughness of the soil surface is described by RMSH, showing a process of first decreasing and then increasing. Under the same conditions, the areas with severe wind erosion are more likely to be damaged. General assumptions are that cropland is the most sensitive area to wind erosion (Zhang et al., 2012; Pierre et al., 2018).

5 Conclusions

In the wind tunnel test, the relative errors of the cumulative wind-driven erosion obtained by the 3D laser scanning technology and the weighing method of the three soil samples were 10.20%, 1.65%, and 7.00%, respectively, and the average relative error was 6.23%. With the increase of wind speed, the microtopography on the undisturbed soil surface first becomes flat and then gradually develops into fine stripes and pits. Then, the pits continue to deepen and widen, and the soil roughness first decreases and then increases. The variation in microtopography during the wind erosion processes is influenced by the soil organic matter, $CaCO_3$ content, and soil hardness. At the initial stage of wind erosion, the ability of soil to resist wind erosion is mainly affected by the soil hardness; that is, the greater the soil hardness, the greater the incoming wind speed it can withstand. With the increase of wind speed, the degree of soil erosion is mainly affected by soil organic matter and $CaCO_3$ content.

Most research methods can only infer the soil erosion processes by calculating the amount material displaced by erosion and the depth of fixed-point erosion. However, 3D laser scanning technology can quantify the microscopic topographic changes of the soil erosion process, which provides new possibilities for further study of wind erosion processes. Moreover, a 3D laser scanner can quickly scan the surface of the target object and obtain 3D coordinates. Thus, it is feasible to apply 3D laser scanning technology to wind erosion monitoring studies by constantly improving the scanning accuracy and controlling the systematic error of measurement. Estimation of a surface roughness index with more accurate and precise point cloud data by laser scanning will be critical to better evaluate and model wind erosion in the future. Wind erosion can be effectively reduced by increasing the soil hardness, soil organic matter, and $CaCO_3$ content by physical and chemical methods. In addition, we believe that wind-driven erosion processes remain the key mechanism controlling desertification.

Acknowledgements

This work is supported by National Natural Science Foundation of China (41871010) and The Second Comprehensive Scientific Expedition to the Qinghai-Tibet Plateau of China (2019QZKK0906).

References

An Z S, Zhang K C, Tan L H, et al. 2017. Application of 3D laster scnner in the sand drift observation. Science of Surveying and Mapping, 42(10): 196–200. (in Chinese)

Asensio C, Weber J, Lozano F J, et al. 2019. Laser-scanner used in a wind tunnel to quantify soil erosion. International Agrophysics, 33(2): 227–232.

Bhutto S L, Miri A, Zhang Y, et al. 2022. Experimental study on the effect of four single shrubs on aeolian erosion in a wind tunnel. CATENA, 212: 106097, doi: 10.1016/j.catena.2022.106097.

Borrelli P, Robinson D A, Panagos P, et al. 2020. Land use and climate change impacts on global soil erosion by water (2015–2070). Proceedings of the National Academy of Sciences, 117(36): 21994–22001.

Carrara P E, Carroll T R. 1979. The determination of erosion rates from exposed tree roots in the Piceance Basin, Colorado. Earth Surface Processes, 4(4): 307–317.

Cheng H, Liu C C, Li J F, et al. 2017. Wind erosion mass variability with sand bed in a wind tunnel. Soil and Tillage Reaearch, 165: 181–189.

Cheng X J, Jin W. 2006. Study on reverse engineering of historical architecture based on 3D laser scanner. Journal of Physics: Conference Series, 48: 843–849.

Chepil W S. 1945. Dynamics of wind erosion: I. Nature of movement of soil by wind. Soil Science, 60(4): 305–320.

Cooke R U, Warren A, Goudie A S. 1993. Desert Geomorphology. Florida: Chemical Rubber Company Press.

Dong M, Yan P, Meng X N, et al. 2018. Effect of calcium carbonate on wind erosion. Research of Soil and Water Conservation, 25(5): 18─23. (in Chinese)

Dunne T, Dietrich W E, Brunengo M J. 1978. Recent and past erosion rates in semi-arid Kenya. Zeitschrift für Geomorphologie, 29: 130–140.

Eitel J U H, Williams C J, Vierling L A, et al. 2011. Suitability of terrestrial laser scanning for studying surface roughness effects on concentrated flow erosion processes in rangelands. CATENA, 87: 398–407.

Fallahzade J, Karimi A, Naderi M, et al. 2020. Soil mechanical properties and wind erosion following conversion of desert to irrigated croplands in central Iran. Soil and Tillage Research, 204: 104665, doi: 10.1016/j.still.2020.104665.

Ferreira C S S, Seifollahi-Aghmiuni S, Destouni G, et al. 2022. Soil degradation in the European Mediterranean region: Processes, status and consequences. Science of the Total Environment, 805: 150106, doi: 10.1016/j.scitotenv.2021.150106.

Guerrero R, Valenzuela J L, Chamizo S, et al. 2021. Multidirectional traps as a new assessment system of soil wind erosion. Scientia Agricola, 79, doi: 10.1590/1678-992X-2020-0342.

Gupta J P, Aggarwal R, Raikhy N P. 1981. Soil erosion by wind from bare sandy plains in western Rajasthan, India. Journal of Arid Environments, 4: 15–20.

Hagen L J. 1991. A wind erosion prediction system to meet user needs. Journal of Soil and Water Conservation, 46(2): 106–111.

Haigh M J. 1977. The use of erosion pins in the study of slope evolution. British Geomorphological Research Group Technical Bulletin, 18: 31–49.

Jaboyedoff M, Oppikofer T, Abellán A, et al. 2012. Use of LIDAR in landslide investigations: a review. Natural Hazards, 61: 5–28.

Jouquet P, Henry-Des-Tureaux T, Bouet C, et al. 2021. Bioturbation and soil resistance to wind erosion in Southern Tunisia. Geoderma, 403: 115198, doi: 10.1016/j.geoderma.2021.115198.

Kardous M, Bergametti G, Marticorena B. 2005. Aerodynamic roughness length related to non-aggregated tillage ridges. Annales Geophysicae, 23(10): 3187–3193.

Kovacs L, Zimmermann A, Brockmann G, et al. 2006. Three-dimensional recording of the human face with a 3D laser scanner. Journal of Plastic Reconstructive and Aesthetic Surgery, 59(11): 1193–1202.

Kuzminsky S C, Gardiner M S. 2012. Three-dimensional laser scanning: potential uses for museum conservation and scientific research. Journal of Archaeological Science, 39: 2744–2751.

Li F R, Zhang H, Zhang T H, et al. 2003. Variations of sand transportation rates in sandy grasslands along a desertification gradient in northern China. CATENA, 53(3): 255–272.

Li F R, Kang L F, Zhang H, et al. 2005. Changes in intensity of wind erosion at different stages of degradation development in grasslands of Inner Mongolia, China. Journal of Arid Environmenta, 62(4): 567–585.

Lyu X, Li X B, Wang H, et al. 2021. Soil wind erosion evaluation and sustainable management of typical steppe in Inner Mongolia, China. Journal of Environmental Management, 277: 111488, doi: 10.1016/j.jenvman.2020.111488.

Mozaffari H, Rezaei M, Ostovari Y. 2021. Soil sensitivity to wind and water erosion as affected by land use in southern Iran. Earth, 2(2): 287–302.

Münch S, Papke N, Leue M, et al. 2022. Differences in the sediment composition of wind eroded sandy soils before and after fertilization with poultry manure. Soil and Tillage Research, 215: 105205, doi: 10.1016/j.still.2021.105205.

Nagihara S, Mulligan K R, Xiong W. 2004. Use of a three-dimensional laser scanner to digitally capture the topography of sand dunes in high spatial resolution. Earth Surface Processes and Landforms, 29(3): 391–398.

Nield J M, Wiggs G F S, Squirrell R S. 2011. Aeolian sand strip mobility and protodune development on a drying beach: examining surface moisture and surface roughness patterns measured by terrestrial laser scanning. Earth Surface Processes and Landforms, 36(4): 513–522.

Nield J M, King J, Wiggs G F S, et al. 2013. Estimating aerodynamic roughness over complex surface terrain. Journal of Geophysical Research: Atmospheres, 118(23): 12948–12961.

Pelletier J D, Sherman D J, Ellis J T, et al. 2015. Dynamics of sediment storage and release on aeolian dune slip faces: A field study in Jericoacoara, Brazil. Journal of Geophysical Research-Earth Surface, 120(9): 1911–1934.

Pierre C, Kergoat L, Hiernaux P, et al. 2018. Impact of agropastoral management on wind erosion in Sahelian croplands. Land Degradation & Development, 29(3): 800–811.

Polig M. 2017. 3D GIS for building archeology–Combining old and new data in a three-dimensional information system in the case study of Lund Cathedral. Studies in Digital Heritage, 1(2): 225–238.

Sansoni G, Trebeschi M, Docchio F. 2009. State-of-the-art and applications of 3D imaging sensors in industry, cultural heritage, medicine, and criminal investigation. Sensors, 9(1): 568–601.

Soudarissanane S, Lindenbergh R, Menenti M, et al. 2011. Scanning geometry: Influencing factor on the quality of terrestrial laser scanning points. ISPRS Journal of Photogrammetry and Remote Sensing, 66(4): 389–399.

Sterk G, Lopez M V, Arrue J L. 1999. Saltation transport on a silt loam soil in Northeast Spain. Land Degradation & Development, 10(6): 545–554.

Sun X H, Miao L C, Wang H X, et al. 2021. Mineralization crust field experiment for desert sand solidification based on enzymatic calcification. Journal of Environmental Management, 287: 112315, doi: 10.1016/j.jenvman.2021.112315.

Tian K L, Wu Y Y, Zhang H L, et al. 2018. Increasing wind erosion resistance of aeolian sandy soil by microbially induced calcium carbonate precipitation. Land Degradation & Development, 29(12): 4271–4281.

Toy T J, Foster G R, Renard K G. 2002. Soil Erosion: Processes, Prediction, Measurement, and Control. New York: John Wiley & Sons.

Wang R D, Chang C P, Peng S, et al. 2013. Estimation on farmland wind-erosion and dust emission amount in Bashang of Hebei province by grain composition contrast. Transactions of the Chinese Society of Agricultural Engineering, 29(21): 108–114. (in Chinese)

Wang R D, Li Q, Chang C P, et al. 2019. Review of field measurement technologies in soil wind erosion. Journal of Desert Research, 39(4): 113–128. (in Chinese)

Wu H Y, Xu X M, Zheng F L, et al. 2018. Gully morphological characteristics in the loess hilly–gully region based on 3D laser scanning technique. Earth Surface Processes and Landforms, 43(8): 1701–1710.

Zhang C L, Song C Q, Wang Z T, et al. 2018. Review and prospect of the study on soil wind erosion process. Advances in Earth Science, 33(1): 27–41. (in Chinese)

Zhang J M, Jia G D, Liu Z Q, et al. 2019. *Populus simonii* Carr. Reduces wind erosion and improves soil properties in Northern China. Forests, 10(4): 315, doi: 10.3390/f10040315.

Zhang Y M, Wang H L, Wang X Q, et al. 2006. The microstructure of microbiotic crust and its influence on wind erosion for a sandy soil surface in the Gurbantunggut Desert of Northwestern China. Geoderma, 132(3–4): 441–449.

Zhang Z, Wieland R, Reiche M, et al. 2012. Identifying sensitive areas to wind erosion in the Xilingele grassland by computational fluid dynamics modelling. Ecological Informatics, 8: 37–47.

Zhao C N, Zhang H B, Wang M, et al. 2021. Impacts of climate change on wind erosion in Southern Africa between 1991 and 2015. Land Degradation & Development, 32(6): 2169–2182.

Zhao L D, Ma X P, Xiang Z F, et al. 2022. Landslide deformation extraction from terrestrial laser scanning data with weighted least squares regularization iteration solution. Remote Sensing, 14(12): 2897, doi: 10.3390/rs14122897.

Zheng B W, Qi S W, Luo G M, et al. 2021. Characterization of discontinuity surface morphology based on 3D fractal dimension by integrating laser scanning with ArcGIS. Bulletin of Engineering Geology and the Environment, 80(3): 2261–2281.

Zheng D H, Shen Y Z, Liu C. 2005. 3D laster scanner and its effect factor analysis of surveying error. Engineering of Surveying and Mapping, 14(2): 32–34. (in Chinese)

Zhou Y, Xiang Z F, Zhang X S, et al. 2022. Mechanical state inversion method for structural performance evaluation of existing suspension bridges using 3D laser scanning. Computer-Aided Civil and Infrastructure Engineering, 37(5): 650–665.